

Supporting Information for

Defect-rich and ultrathin CoOOH nanolayers as highly efficient oxygen evolution catalysts for photoelectrochemical water splitting

BeibeiZhang,^{†,§} Xiaojuan Huang,[†] Hongyan Hu,[†] Lingjun Chou^{*†}, and Yingpu Bi^{*†}

[†]. State Key Laboratory for Oxo Synthesis & Selective Oxidation, National Engineering Research Center for Fine Petrochemical Intermediates, Lanzhou Institute of Chemical Physics, CAS, Lanzhou, Gansu, 730000, China

[§]. University of Chinese Academy of Sciences, Beijing 100049, China

E-mail: yingpubi@licp.cas.cn

Experiment section

Chemical reagents and Instruments

Potassium iodide (KI), bismuth nitrate pentahydrate ($\text{Bi}(\text{NO}_3)_3 \cdot 5\text{H}_2\text{O}$, 99%), p-benzoquinone, vanadium acetylacetonate ($\text{VO}(\text{acac})_2$), dimethylsulfoxide (DMSO), ethyl alcohol, nitric acid (HNO_3), sodium sulfate (Na_2SO_4 , 99%), sodium sulfite (Na_2SO_3 , 99%), cobalt sulfate (CoSO_4 , 99%), and sodium hydroxide (NaOH , 99%) were obtained from Sinopharm Chemical Reagent Co., Ltd. Fluorine-doped Tin Oxide (FTO) coated glasses as substrates were purchased from Zhuhai Kaivo Electronic Components Co., Ltd. China. Deionized water with a resistivity of $18.25 \text{ M}\Omega \cdot \text{cm}$ was used in all reactions.

Scanning electron microscope measures were carried out on a field-emission scanning electron microscope (SEM, JSM-6701F, JEOL) operated at an accelerating voltage of 5 kV. Transmission electron microscopy (TEM) measurements were carried out by using a FEI Tecnai TF20 microscope operated at 200 kV. The crystalline structure of the samples was identified by X-ray diffraction analysis (XRD, X'Pert PRO) using $\text{Cu K}\alpha$ radiation at 50 kV and 50 mA. The elemental composition was determined by X-ray photoelectron spectroscopy (XPS, Kratos Axis Ultra DLD). The plasma processing was carried out by a plasma cleaner (PDC-36G, Hefei Kejing Materials Technology Co., Ltd)

Preparation of nanoporous BiVO_4 photoanodes.

Nanoporous BiVO_4 photoanodes were fabricated by an electrodeposition method.^[6] 3.32 g KI was dissolved into 50 mL deionized water, followed by adding 0.9701 g $\text{Bi}(\text{NO}_3)_3 \cdot 5\text{H}_2\text{O}$, and then adjusted its pH to 1.7 by adding HNO_3 . This solution was mixed with 20 mL of ethanol containing 0.23 M p-benzoquinone, and was vigorously stirred for a few minutes. A typical three-electrode cell was used for electrodeposition. A FTO working electrode (WE), an Ag/AgCl (4 M KCl) reference electrode (RE), and a platinum counter electrode (CE) were used. Cathodic deposition was performed potentiostatically at -0.1 V vs. Ag/AgCl for 3 min at room temperature. Then, 0.2 mL DMSO solution containing 0.2 M $\text{VO}(\text{acac})_2$ was placed on the BiOI electrode (1 cm \times 1.3 cm), and was heated in a muffle furnace (HF-Kejing Furnace, KSL-1100X) at 450 °C (ramping rate=2 °C/min) for 2 h in air to convert BiOI to BiVO_4 . Excess V_2O_5 in the BiVO_4 electrodes was removed by soaking them in 1M NaOH solution for 30 min with gentle stirring. The resulting pure BiVO_4 electrodes were rinsed with DI water and dried in air.

Preparation of CoOOH/BiVO₄ and Ar-plasma treatment

The CoOOH/BiVO₄ was prepared by solution impregnation. The BiVO₄ photoanodes were immersed in a mixed solution of 0.1M CoSO₄ and 0.1M NaOH with a ratio of 1:1 for 30 min and then washed with DI water and dried at 60°C. The photoanodes were treated by Ar or O₂ plasma with a medium power of 10.5 W and pressure of 300 Pa for different time.

Photoelectrochemical measurements.

The photoelectrochemical properties were measured by an electrochemical analyzer (CHI660D) in a standard three-electrode system. The illumination source was a simulated sunlight AM 1.5G (100 mW/cm²), and a 0.2 M Na₂SO₄ solution (pH=7) was used as the electrolyte. Photocurrent vs. voltage (*J-V*) characteristics were recorded by scanning the potential from -0.6 to 1.0 V (vs. Ag/AgCl) with a scan rate of 10 mV s⁻¹ using a Jaisle IMP 88 PC potentiostat. The measured potentials vs. Ag/AgCl were converted to the reversible hydrogen electrode (RHE) scale using the relationship $E_{\text{RHE}} = E_{\text{Ag/AgCl}} + 0.059\text{pH} + E_{\text{Ag/AgCl}}^0$, where $E_{\text{Ag/AgCl}}$ is the experimentally measured potential and $E_{\text{Ag/AgCl}}^0 = 0.209$ V (vs Ag/AgCl) at 25 °C. The incident photon to current efficiency (IPCE) was determined using a full solar simulator (Newport, Model 9600, 300W Xe arc lamp) and a motorized monochromator (Oriel Cornerstone 130 1/8 m). IPCE was measured at 1.23 V_{RHE} in 0.2 M Na₂SO₄ solution using the same three-electrode setup described above for photocurrent measurements. IPCE was calculated as follow:

$$\text{IPCE} = 1240 \times I (\text{mA/cm}^2) / (P_{\text{light}} (\text{mW/cm}^2) \times \lambda (\text{nm}))$$

Where *I* is the measured photocurrent density at specific wavelength, λ is the wavelength of incident light, and P_{light} is the measured light power density at that wavelength. Supposing 100% Faradaic efficiency, the applied bias photon-to-current efficiency (ABPE) was calculated by following equation:

$$\text{ABPE} = I (\text{mA/cm}^2) \times (1.23 - V_{\text{bias}} (\text{V})) / P_{\text{light}} (\text{mW/cm}^2)$$

Where *I* is the photocurrent density, V_{bias} is the applied potential, P_{light} is the incident illumination power density (100 mW cm⁻²). The electrochemical impedance spectroscopy (EIS) Nyquist plots were obtained at 1.23 V (vs. RHE) with small AC amplitude of 10 mV in the frequency range of 10⁻² to 10⁵ Hz. The measured spectra were fitter with Zview. Photoelectrochemical H₂ evolution was studied in 0.2 M Na₂SO₄ by an on-line device. Evolved H₂ gas was collected and measured according to the standard H₂ evolution curve by a gas chromatograph (GC-2014C, Shimadzu).

The surface charge separation sufficiency (η_{surface}) was calculated using the equation:

$$\eta_{\text{surface}} = J_{\text{water}}/J_{\text{sulfite}}$$

Additional Figures and Discussions

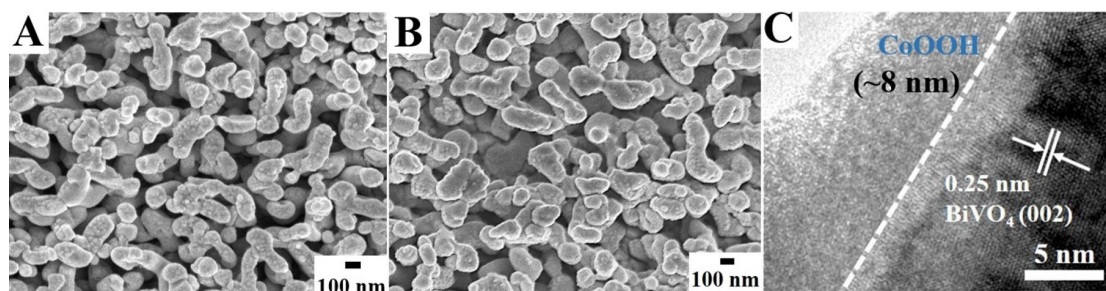


Figure S1. SEM images of the pristine BiVO_4 (A) and $\text{CoOOH}/\text{BiVO}_4$ (B); (C) HR-TEM image of $\text{CoOOH}/\text{BiVO}_4$.

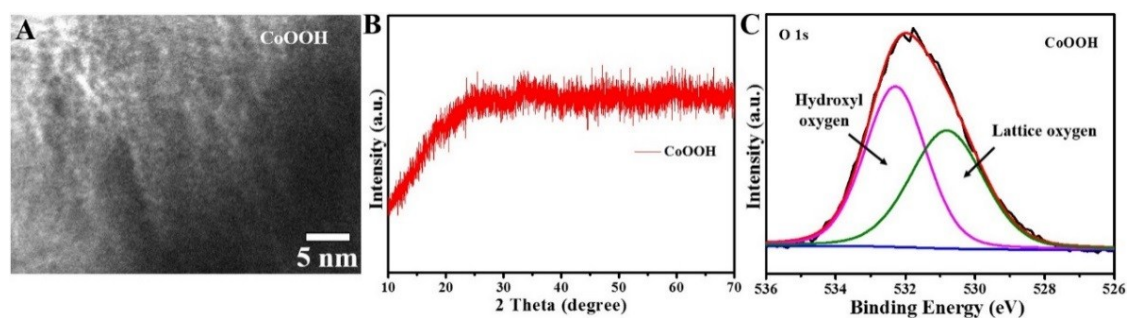


Figure S2. HR-TEM image (A), XRD pattern (B) and XPS high-resolution spectra of O 1s (C) of CoOOH .

Additional discussions

As shown in the HR-TEM images (Figure 1C and Figure S1C), the CoOOH nanolayer loading on the surfaces of BiVO_4 photoanodes should be the amorphous structure. To further confirm this speculation, the pure Co-based nanofilms obtained under the same condition were studied by HR-TEM, XRD, and XPS. As shown in Figure S2A and S2B, both HR-TEM and XRD results clearly confirmed their amorphous structure. Moreover, the XPS spectra shown in Figure S2C clearly demonstrated that the O 1s peak could be well fitted into two oxygen species located at 530.8 and 532.3 eV, respectively, which could be well indexed to the lattice oxygen and hydroxyl oxygen. On the basis of above results, it can be concluded that the CoOOH nanofilms with an amorphous structure have been formed on the BiVO_4 photoanodes.

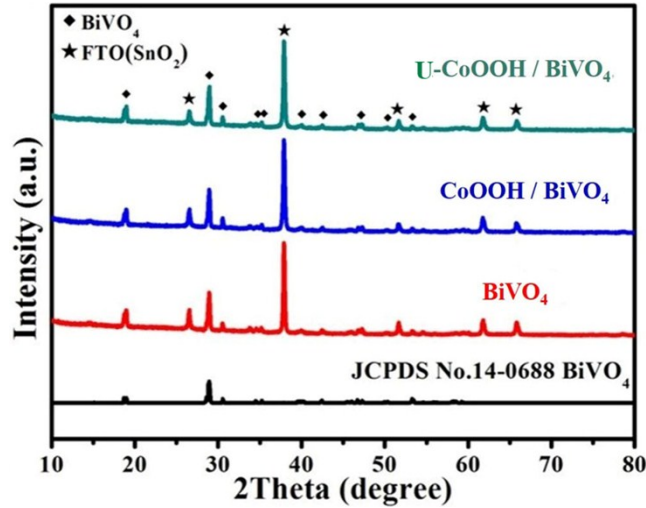


Figure S3. The XRD patterns of different photoanodes.

Additional discussions

The XRD patterns of BiVO_4 based CoOOH samples (Figure S3) exhibit that all the characteristic peaks are corresponding to the BiVO_4 (JCPDS No.14-0688), except for the diffraction peaks of SnO_2 from the FTO substrate, and no characteristic peak of CoOOH was detected, which is due to the amorphous structure of CoOOH on the surface of BiVO_4 .

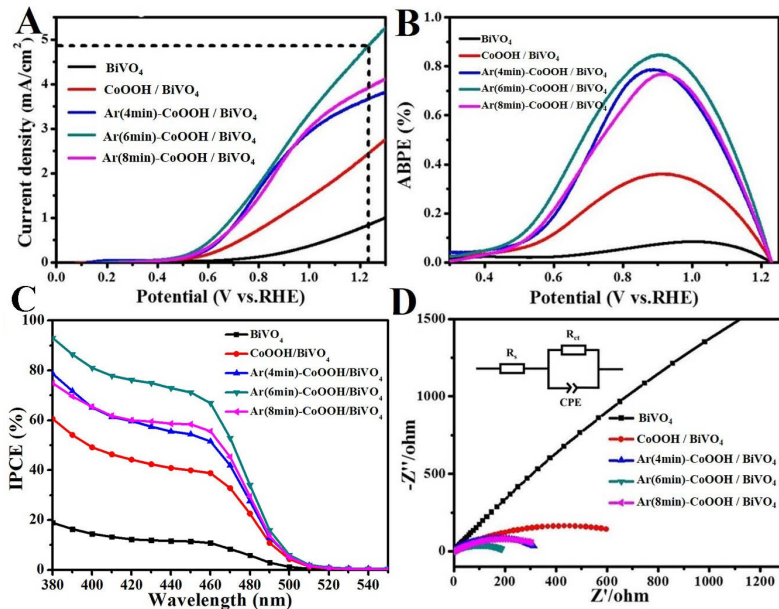


Figure S4. (A) Photocurrent density versus applied potential curves, (B) applied bias photon to current efficiencies (ABPEs), (C) incident photon to current conversion efficiencies (IPCEs) at $1.23 V_{\text{RHE}}$, and (D) electrochemical impedance spectroscopy (EIS) of BiVO_4 , $\text{CoOOH}/\text{BiVO}_4$, $\text{Ar}(4\text{min})\text{-CoOOH}/\text{BiVO}_4$, $\text{Ar}(6\text{min})\text{-CoOOH}/\text{BiVO}_4$ and $\text{Ar}(8\text{min})\text{-CoOOH}/\text{BiVO}_4$ photoanodes. All the measurements were carried out in $0.2\text{M Na}_2\text{SO}_4$ and AM 1.5G (100 mW cm^{-2}).

Additional discussions

To investigate the PEC performance of the as-prepared photoanodes, the PEC water oxidation measurements were carried out in a three-electrode system, 0.2M Na₂SO₄ electrolyte and AM 1.5G (100 mW cm⁻²) simulated sunlight conditions. As shown in Figure S4, it can be clearly seen that the photocurrent densities of all CoOOH/BiVO₄ photoanodes treated by Ar plasma for different time were enhanced, and the optimum performance of the photoanode was managed for 6 minutes, recorded as U-CoOOH/BiVO₄, which could attain a photocurrent density of 4.9 mA cm⁻² at 1.23V_{RHE}, indicating that the Ar plasma plays an important role in enhancing the PEC performance and the photocurrent densities could be changed by adjusting Ar plasma treatment time. Moreover, the applied bias photon to current efficiencies (ABPE) and the incident photon to electron conversion efficiency (IPCE) results (Figures S4B and C) confirm that the Ar plasma treatment could effectively improve the PEC performances of CoOOH/BiVO₄ photoanodes. Additionally, from Figure S4C, it can be observed that even below the wavelength of 420nm, the plasma-exfoliation of CoOOH nanolayers could also significantly improve the photo-conversion efficiency. Meanwhile, the electrochemical impedance spectroscopy (EIS, Figure S4D) clarifies that the Ar plasma treating could significantly enhance the conductivity and facilitate interface charge transfer between CoOOH and BiVO₄.

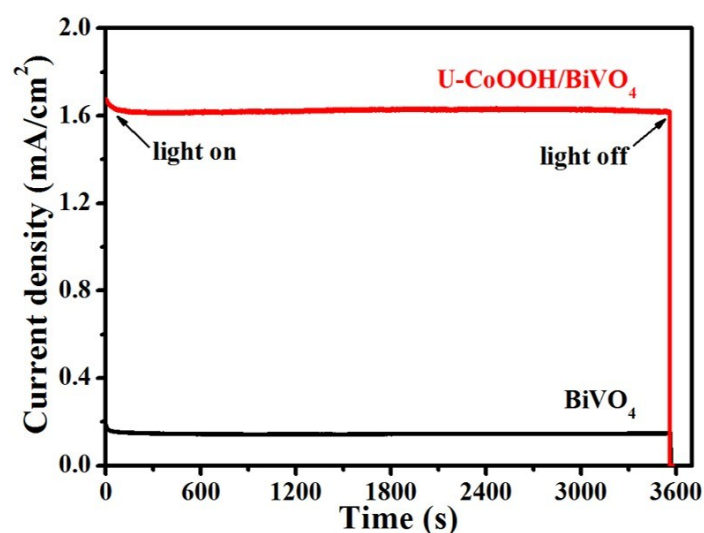


Figure S5. I-t curves for BiVO₄ and U-CoOOH/BiVO₄ photoanodes measured at 0.8 V_{RHE} in 0.2M Na₂SO₄ under AM 1.5G (100 mW cm⁻²).

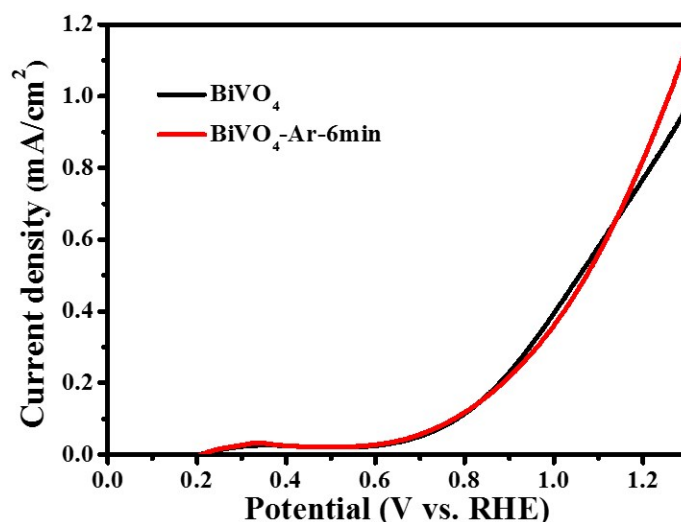


Figure S6. J-V curves for BiVO₄ photoanodes treated by Ar plasma.

Table S1. The fitted results of EIS data using the equivalent circuit in Figure 2D.

Samples	R_s/Ω	R_{ct}/Ω
BiVO ₄	31.15±0.3	12546±751.9
CoOOH / BiVO ₄	27.37±0.3	517.2±7.149
U-CoOOH / BiVO ₄	31.67±0.4	205.6±4.84

Additional discussions

The impedance data (Table S1) is obtained by fitting the equivalent circuit model shown in Figure 2D. Where R_s represents the resistance across the semiconductor/electrolyte interface and R_{ct} represents the resistance in the different photoanodes. Compared with the pristine BiVO₄, the R_{ct} of CoOOH/BiVO₄ decreased significantly (from 12546 Ω to 517.2 Ω). After Ar plasma processing the CoOOH/BiVO₄ for 6 min, the R_{ct} further decreased to 205.6 Ω . The R_s of the three photoanodes is basically no change.

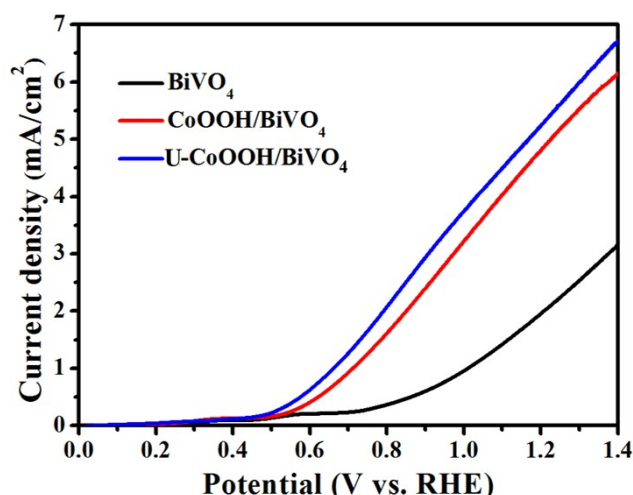


Figure S7. J-V curves measured with 0.2 M Na₂SO₄ with Na₂SO₃ of BiVO₄, CoOOH/BiVO₄ and U-CoOOH/BiVO₄ photoanodes.

Additional discussions

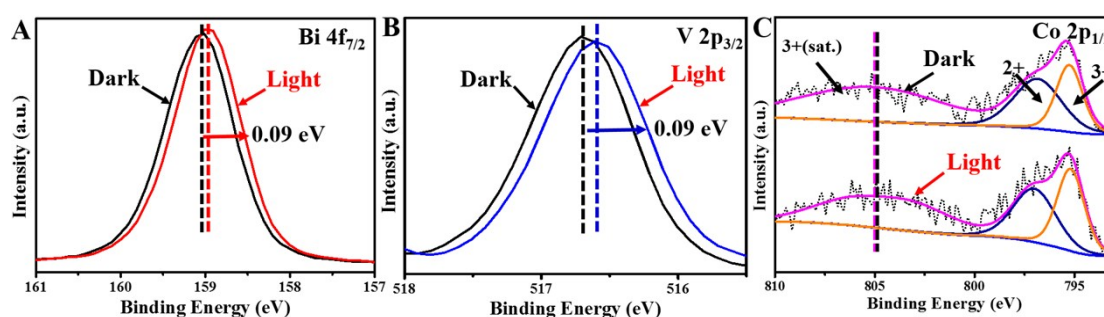
The J-V curves shown in Figure S7 for sulfite oxidation display that the photocurrent densities of BiVO₄, CoOOH/BiVO₄ and U-CoOOH/BiVO₄ photoanodes have increased, demonstrating that the oxidation of sulfite is thermodynamically and kinetically more favorable than water oxidation. According to the J-V results, the U-CoOOH/BiVO₄ photoanode exhibits a charge separation efficiency of 89% at 1.23 V_{RHE}, which is much higher than both BiVO₄ (39%) and CoOOH/BiVO₄ (48%) samples, illustrating that the Ar-plasma treatment on CoOOH cocatalyst could efficiently enhance the surface charge separation as well as interfacial hole transfer and trapping.

Table S2. Atomic ratios of O_L and O_V from XPS spectrum

Samples	Atomic ratios of O _L	Atomic ratios of O _V
BiVO ₄	68.8%	31.2%
CoOOH / BiVO ₄	48.6%	51.4%
U-CoOOH / BiVO ₄	35.2%	64.8%
O ₂ -CoOOH / BiVO ₄	44%	56%

Table S3. The fitted results of EIS data using the equivalent circuit in Figure 3D.

Samples	R_s/Ω	R_{ct}/Ω
U-CoOOH / BiVO ₄	31.67±0.4	205.6±4.84
O ₂ (3min)- U-CoOOH / BiVO ₄	29.97±0.5	394.3±8.73
O ₂ (5min)- U-CoOOH / BiVO ₄	29.68±0.3	480.5±6.91
O ₂ (7min)- U-CoOOH / BiVO ₄	31.1 ± 0.3	542.2±8.46

**Figure S8.** ISI-XPS spectra of Bi 4f (A), V 2p (B) and Co 2p (C) of CoOOH/BiVO₄ photoanodes.**Table S4.** The ratio of Co²⁺/Co³⁺ species from ISI-XPS spectra in Figure 4D.

Samples	Co ²⁺ (peak area)	Co ³⁺ (peak area)	Co ²⁺ /Co ³⁺
U-CoOOH/BiVO ₄	Dark: 2261.236	Dark: 949.0627	Dark: 2.38
	Light: 1875.639	Light: 1361.731	Light: 1.38

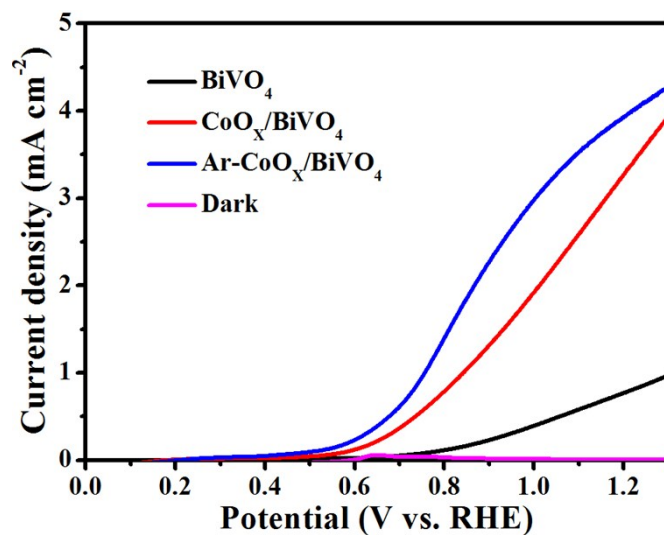


Figure S9. J-V curves for CoO_x/BiVO₄ photoanodes treated by Ar plasma.

Additional discussions

The effect of Ar plasma treatment on CoO_x cocatalyst has also been studied shown in Figure S9. After Ar plasma treating, the photocurrent density of CoO_x/BiVO₄ improved compared with un-treated sample, indicating that this strategy is also effective for other cocatalysts modified photoanode materials, which may provide a feasible and universal technique for building the highly efficient solar water splitting systems.

Table S5 Comparison of our photoanode to other cocatalysts modified BiVO₄ photoanodes

Photoanode	Photocurrent	Condition	Electrolyte	Ref.
Co-Pi/W/BiVO ₄	1.4 mA/cm ²	1.23V vs. RHE AM1.5,100mW/cm ²	Phosphate (pH 8)	1
CoO _x /BiVO ₄	1.49 mA/cm ²	1.23V vs. RHE AM1.5,100mW/cm ²	KOH (pH 13)	2
Co-Pi/BiVO ₄	1.7 mA/cm ²	1.23V vs. RHE AM1.5,100mW/cm ²	0.5 M K ₂ SO ₄ (pH 5.6)	3
Co ₃ O ₄ /BiVO ₄	2.71 mA/cm ²	1.23V vs. RHE AM1.5,100mW/cm ²	Phosphate (pH 7)	4
BiVO ₄ /FeCoO _x	4.82 mA/cm ²	1.23V vs. RHE AM1.5,100mW/cm ²	1 M potassium borate (pH 9.5)	5
BiVO ₄ /FeOOH/NiOOH	4.5 mA/cm ²	1.23V vs. RHE AM1.5,100mW/cm ²	Phosphate (pH 7)	6
BiVO ₄ /β-FeOOH	4.3 mA/cm ²	1.23V vs. RHE AM1.5,100mW/cm ²	0.2 M Na ₂ SO ₄ (pH 7)	7
BL-BiVO ₄ /NiFeO _x -B ₁	3.1 mA/cm ²	1.23V vs. RHE AM1.5,100mW/cm ²	0.1 M K ₂ B ₄ O ₇ (pH 9.6)	8
BiVO ₄ /NiO _x -400°C	2.44 mA/cm ²	1.23V vs. RHE AM1.5,100mW/cm ²	0.5 M Na ₂ SO ₄ (pH 6.8)	9
U-CoOOH/BiVO ₄	4.9 mA/cm ²	1.23V vs. RHE AM1.5,100mW/cm ²	0.2 M Na ₂ SO ₄ (pH 7)	This work

Additional discussions

The reported PEC activities of BiVO₄ photoanodes with various OER cocatalysts have been listed in the Table S5, clearly indicating that the photo-conversion efficiency of U-CoOOH/BiVO₄ is higher than that of the reported photoanodes.

Reference

- [1] D. K. Zhong, S. Choi, D. R. Gamelin, *J. Am. Chem. Soc.* 2011, **133**, 18370-18377.
- [2] M. F. Lichterman, M. R. Shaner, S. G. Handler, B. S. Brunschwig, H. B. Gray, N. S. Lewis, J. M. Spurgeon, *J. Phys. Chem. Lett.* 2013, **4**, 4188-4191.
- [3] F. F. Abdi, R. Krol, *J. Phys. Chem. C* 2012, **116**, 9398-9404.
- [4] X. Chang, T. Wang, P. Zhang, J. Zhang, A. Li, J. Gong, *J. Am. Chem. Soc.* 2015, **137**, 8356-8359.
- [5] S. Wang, T. He, J-H. Yun, Y. Hu, M. Xiao, A. Du, L. Wang, *Adv. Funct. Mater.* 2018, **28**, 1802685.
- [6] T. W. Kim, K. S. Choi, *Science* 2014, **343**, 990-994.
- [7] B. Zhang, L. Wang, Y. Zhang, Y. Ding, Y. Bi, *Angew. Chem. Int. Ed.* 2018, **57**, 2248-2252.
- [8] M. Huang, C. Li, L. Zhang, Q. Chen, Z. Zhen, Z. Li, H. Zhu, *Adv. Energy Mater.* 2018, **8**, 1802198.
- [9] M. Zhang, R. P. Antony, S. Y. Chiam, F. F. Abdi, L. H. Wong, *ChemSusChem* 2018, DOI: 10.1002/cssc.201801780.